



## Redistribution of lamina-associated domains reshapes binding of pioneer factor FOXA2 in development of nonalcoholic fatty liver disease

Xiaolong Wei, Megan A. Murphy, Nihal A. Reddy, et al.

*Genome Res.* 2022 32: 1981-1992 originally published online December 15, 2022  
Access the most recent version at doi:[10.1101/gr.277149.122](https://doi.org/10.1101/gr.277149.122)

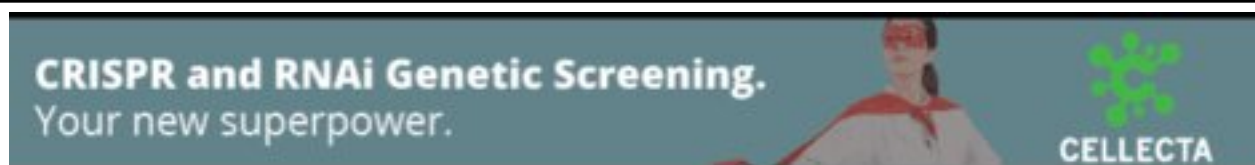
---

**References** This article cites 38 articles, 3 of which can be accessed free at:  
<http://genome.cshlp.org/content/32/11-12/1981.full.html#ref-list-1>

**Open Access** Freely available online through the *Genome Research* Open Access option.

**Creative Commons License** This article, published in *Genome Research*, is available under a Creative Commons License (Attribution-NonCommercial 4.0 International), as described at <http://creativecommons.org/licenses/by-nc/4.0/>.

**Email Alerting Service** Receive free email alerts when new articles cite this article - sign up in the box at the top right corner of the article or [click here](#).



---

To subscribe to *Genome Research* go to:  
<https://genome.cshlp.org/subscriptions>

## Research

# Redistribution of lamina-associated domains reshapes binding of pioneer factor FOXA2 in development of nonalcoholic fatty liver disease

Xiaolong Wei,<sup>1</sup> Megan A. Murphy,<sup>1</sup> Nihal A. Reddy,<sup>1</sup> Yi Hao,<sup>1</sup> Taylor G. Eggertsen,<sup>2</sup> Jeffrey J. Saucerman,<sup>2</sup> and Irina M. Bochkis<sup>1</sup>

<sup>1</sup>Department of Pharmacology, <sup>2</sup>Department of Biomedical Engineering, University of Virginia, Charlottesville, Virginia 22908, USA

Nonalcoholic fatty liver disease (NAFLD) is highly prevalent in type 2 diabetes mellitus and the elderly, impacting 40% of individuals over 70. Regulation of heterochromatin at the nuclear lamina has been associated with aging and age-dependent metabolic changes. We previously showed that changes at the lamina in aged hepatocytes and laminopathy models lead to redistribution of lamina-associated domains (LADs), opening of repressed chromatin, and up-regulation of genes regulating lipid synthesis and storage, culminating in fatty liver. Here, we test the hypothesis that change in the expression of lamina-associated proteins and nuclear shape leads to redistribution of LADs, followed by altered binding of pioneer factor FOXA2 and by up-regulation of lipid synthesis and storage, culminating in steatosis in younger NAFLD patients (aged 21–51). Changes in nuclear morphology alter LAD partitioning and reduced lamin B1 signal correlate with increased FOXA2 binding before severe steatosis in young mice placed on a western diet. Nuclear shape is also changed in younger NAFLD patients. LADs are redistributed and lamin B1 signal decreases similarly in mild and severe steatosis. In contrast, FOXA2 binding is similar in normal and NAFLD patients with moderate steatosis and is repositioned only in NAFLD patients with more severe lipid accumulation. Hence, changes at the nuclear lamina reshape FOXA2 binding with progression of the disease. Our results suggest a role for nuclear lamina in etiology of NAFLD, irrespective of aging, with potential for improved stratification of patients and novel treatments aimed at restoring nuclear lamina function.

[Supplemental material is available for this article.]

The prevalence of metabolic disease is rising rapidly in the United States and the rest of the world. Metabolic syndrome, a collection of symptoms that are associated with increased risk of developing type 2 diabetes mellitus (T2D), affects 60% of the U.S. population over 50. Nonalcoholic fatty liver disease (NAFLD) is highly prevalent in T2D (Portillo-Sanchez et al. 2015) and the elderly, impacting 40% of individuals over 70 (Gan et al. 2011).

Mutations in *LMNA*, encoding one of nuclear lamina-associated proteins lamin A/C, result in nuclear lamina dysfunction and cause the premature aging syndrome Hutchinson–Gilford progeria (HGPS). Additionally, *LMNA* mutations lead to partial lipodystrophy, a condition associated with insulin-resistant diabetes, hypertriglyceridemia, renal disease, cardiomyopathy, and hepatic steatosis (Shackleton et al. 2000). Multiple enzymes modulating covalent modifications to lysine 9 of histone 3 (H3K9), the mark associated with heterochromatin in lamina-associated domains (LADs) (Guelen et al. 2008), have been linked to fatty liver, hyperlipidemia, diabetes, diabetic nephropathy, and obesity (Picard et al. 2002; Villeneuve et al. 2008; Tateishi et al. 2009; Sun et al. 2012; Wang et al. 2013, 2018).

Changes at the nuclear lamina have been observed in several mouse models of NAFLD, including aged mouse and *Zmpste24* mutants (Whitton et al. 2018), a laminopathy model (Varela et al. 2005). We previously showed that changes in the expression of lamina-associated proteins and shape of the nucleus in aged fatty

hepatocytes and *Zmpste24*-deficient livers are linked to altered binding of pioneer factor FOXA2, enabling an increase in chromatin accessibility and derepression of expression of lipid metabolism targets regulated by nuclear receptors NR1H3 (also known as LXR alpha) and PPAR (Whitton et al. 2018). Hence, genetic laminopathy causes a fatty liver phenotype and changes in heterochromatin that are completely reproduced in aging liver.

Several studies have reported changes at the nuclear lamina in patients with metabolic disease and NAFLD. Genetic variants in the nuclear lamina-related genes *ZMPSTE24* and *TMPO*, which encode the lamina-associated polypeptide-2 (LAP2), have been associated with NAFLD (Brady et al. 2018), and changes in nuclear morphology parameters have been observed in NAFLD patients (Segovia-Miranda et al. 2019). In addition, a high incidence of laminopathy was found among patients with metabolic syndrome (Dutour et al. 2011). Cells from these individuals presented with dysmorphic nuclear shape and abnormal nuclear distribution of lamin A. These patients, in addition to being younger, also had hypertriglyceridemia and elevated alanine aminotransferase (ALT) levels compared with other metabolic syndrome patients, suggesting liver dysfunction. Furthermore, a heterozygous mutation in *ZMPSTE24* was found in a patient with severe metabolic syndrome (Galant et al. 2016). Fibroblasts from this individual showed nuclear shape abnormalities, and the patient presented with early onset T2D, liver steatosis, and hypertriglyceridemia. Collectively, these observations support the hypothesis that changes at the nuclear lamina promote hepatic fat accumulation

**Corresponding author:** [imb3q@virginia.edu](mailto:imb3q@virginia.edu)

Article published online before print. Article, supplemental material, and publication date are at <https://www.genome.org/cgi/doi/10.1101/gr.277149.122>. Freely available online through the *Genome Research* Open Access option.

© 2022 Wei et al. This article, published in *Genome Research*, is available under a Creative Commons License (Attribution-NonCommercial 4.0 International), as described at <http://creativecommons.org/licenses/by-nc/4.0/>.

in humans. In this study, we test the hypothesis that change in expression of lamina-associated proteins and nuclear shape leads to redistribution of LADs, leading to the altered binding of pioneer factor FOXA2, derepression of nuclear receptor-dependent transcription, and development of hepatic steatosis in a diet-induced mouse model of NAFLD and younger NAFLD patients (aged 21–51).

## Results

### Nuclear lamina changes in diet-induced fatty liver

We previously showed that changes at the lamina in aged hepatocytes and laminopathy models lead to redistribution of LADs, opening of repressed chromatin, and up-regulation of genes regulating lipid synthesis and storage, culminating in fatty liver (Whitton et al. 2018). To test the hypothesis that changes at the nuclear lamina drive development of hepatic steatosis in NAFLD, we used a diet-induced mouse model of NAFLD (study design in Fig. 1A, mouse; Fig. 1B, NAFLD patients). Heterozygous C57BL/6J (B6)/129S1/SvImJ (S129) 8- to 12-wk-old mice were fed a western diet (WD; 42% kcal from fat and containing 0.1% cholesterol; Harlan TD.88137) with ad libitum consumption of glucose and fructose (SW; 23.1 g/L d-fructose +18.9 g/L d-glucose) (Asgharpour et al. 2016). The nuclear shape in livers of mice on WD, detected by LAMIN B1 immunofluorescence and DAPI fluorescence staining, started diverging at 8 wk before substantial lipid accumulation (mild steatosis) (Fig. 2A, top panel) and was completely distorted by 12 wk, when steatosis was severe (Fig. 2A, hematoxylin & eosin staining, bottom panel; Supplemental Fig. S1). The circularity of nuclei was significantly changed in livers of mice on WD at 12 wk (Supplemental Fig. S1), correlating with decreased expression of lamin B1 (*LMNB1*) (Fig. 2B). Then, we profiled LADs using lamin B1 ChIP-seq in livers of mice on normal

diet (ND) and WD. The number of LADs is comparable (1396 ND vs. 1508 western diet 8 wk [WD8]), and the lamin B1 ChIP-seq signal is slightly decreased at WD8 (Fig. 2C–E). The number of LADs is greatly reduced (1386 ND vs. 141 western diet 12 wk [WD12]), and lamin B1 ChIP-seq signal is decreased significantly in WD12 (Fig. 2C–E). Next, we performed scanning motif of positional weight matrices in the JASPAR and TRANSFAC databases in LADs in ND (left), WD8 (middle), and WD12 (right). PscanChIP identified highly enriched consensus sites for A/T-rich sequences, including TATA box ( $P$ -value  $< 8.9 \times 10^{-108}$ ) and the forkhead motif bound by Fox transcription factors ( $P$ -value  $< 8.8 \times 10^{-93}$ ) in ND, forkhead consensus ( $P$ -value  $< 4.9 \times 10^{-106}$ ) and nuclear receptor half-site ( $P$ -value  $< 6.7 \times 10^{-32}$ ) in WD8, and GATA consensus ( $P$ -value  $< 1.4 \times 10^{-8}$ ) and A/T-rich TATA box motif ( $P$ -value  $< 1.8 \times 10^{-5}$ ) in WD12 (Fig. 2F).

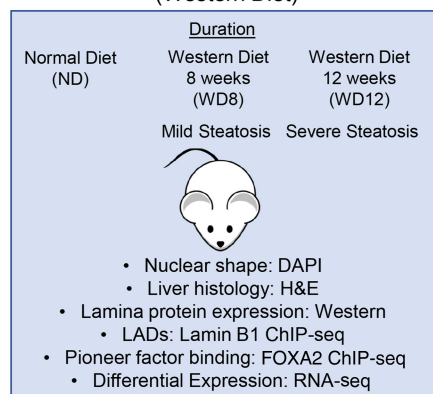
### FOXA2 binding increases in diet-induced fatty liver

Because we found the forkhead motif to be enriched in LADs in ND and WD8 and have shown that redistribution of LADs in aging and laminopathy models of fatty liver led to altered FOXA2 binding (Whitton et al. 2018), we performed FOXA2 ChIP-seq in livers of mice on ND and WD. PeakSeq, the algorithm we use to call peaks, is sensitive to the size of the alignment file (Rozowsky et al. 2009). Hence, we down-sampled all conditions to the same number of reads. FOXA2 occupancy increases in WD8 (6985 sites in ND, 5189 in WD8, 11,191 in WD12) (Fig. 3A), whereas FOXA2 protein expression at either WD8 or WD12 remains constant (Fig. 3B). Hence, changes in FOXA2 binding are independent of its expression. Although we called around 5000 FOXA2 binding sites in WD8, there appear to be additional sites on the heatmap (Fig. 3A) that were not called because they did not reach the threshold. FOXA2 binding at WD8, when steatosis is mild, is driven by bile

acid activation of NR1H4 (also known as FXR) (Figs. 3C, 4E). In contrast, WD12 resembles the severe steatosis observed in *Zmpste24* mutants, a laminopathy model (Mariño et al. 2008). At 12 wk on WD, acute induction of FOXA2 binding by nuclear receptor ligands has long finished, and altered FOXA2 occupancy is influenced only by changes at the lamina (Fig. 2A; Supplemental Fig. S1).

Next, we mapped FOXA2-bound sites to closest genes using GREAT (McLean et al. 2010) and selected 750 genes that mapped closest to the transcription start site (TSS) for pathway analysis with Enrichr (Fig. 3C; Kuleshov et al. 2016). Overrepresented pathways included “bile acid and bile salt biosynthesis” and “composition of lipid particles” for both FOXA2 sites in ND and WD8. Genes regulating lipid metabolism and ER quality control were among FOXA2 targets in ND, consistent with our previous reports (Bochkis et al. 2008, 2009, 2012). Pathways including “statin inhibition of cholesterol production” and “growth hormone signaling pathway” were enriched in FOXA2 sites bound in WD8. A previous study reported that the deletion of a

#### A Diet-Induced Model of NAFLD in Mice (Western Diet)



#### B Nonalcoholic Fatty Liver Disease (NAFLD)

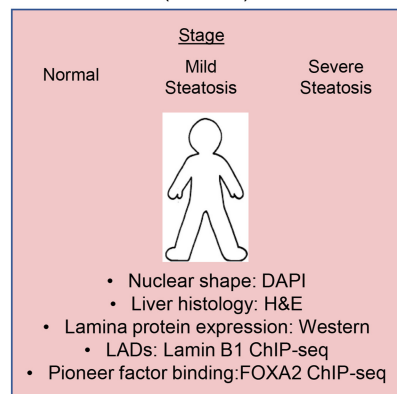


**Figure 1.** Study design. (A) We used a diet-induced mouse model of NAFLD (Asgharpour et al. 2016). Heterozygous 8- to 12-wk-old C57BL/6J (B6)/129S1/SvImJ (S129) mice were fed a western diet (WD; 42% kcal from fat and containing 0.1% cholesterol; Harlan TD.88137) with ad libitum consumption of glucose and fructose (SW; 23.1 g/L d-fructose +18.9 g/L d-glucose) for 8 wk (WD8) and 12 wk (WD12), when the animals developed mild and severe steatosis, respectively. Nuclear shape was determined by DAPI staining, liver histology by hematoxylin and eosin (H&E) staining, and expression of lamina proteins by western blot. Lamin B1 and FOXA2 ChIP-seq were performed to identify LADs and pioneer factor binding. Differential expression on different diets was determined by RNA-seq. (B) Liver tissue samples from donors (three healthy, three NAFLD with mild steatosis, and three NAFLD with severe steatosis; healthy, 26–45 yr old; NAFLD, 21–51 yr old) were obtained from Sekisui XenoTech Biobank. Nuclear shape was determined by DAPI staining, liver histology by H&E staining, and expression of lamina proteins by western blot. Lamin B1 and FOXA2 ChIP-seq were performed to identify LADs and pioneer factor binding.

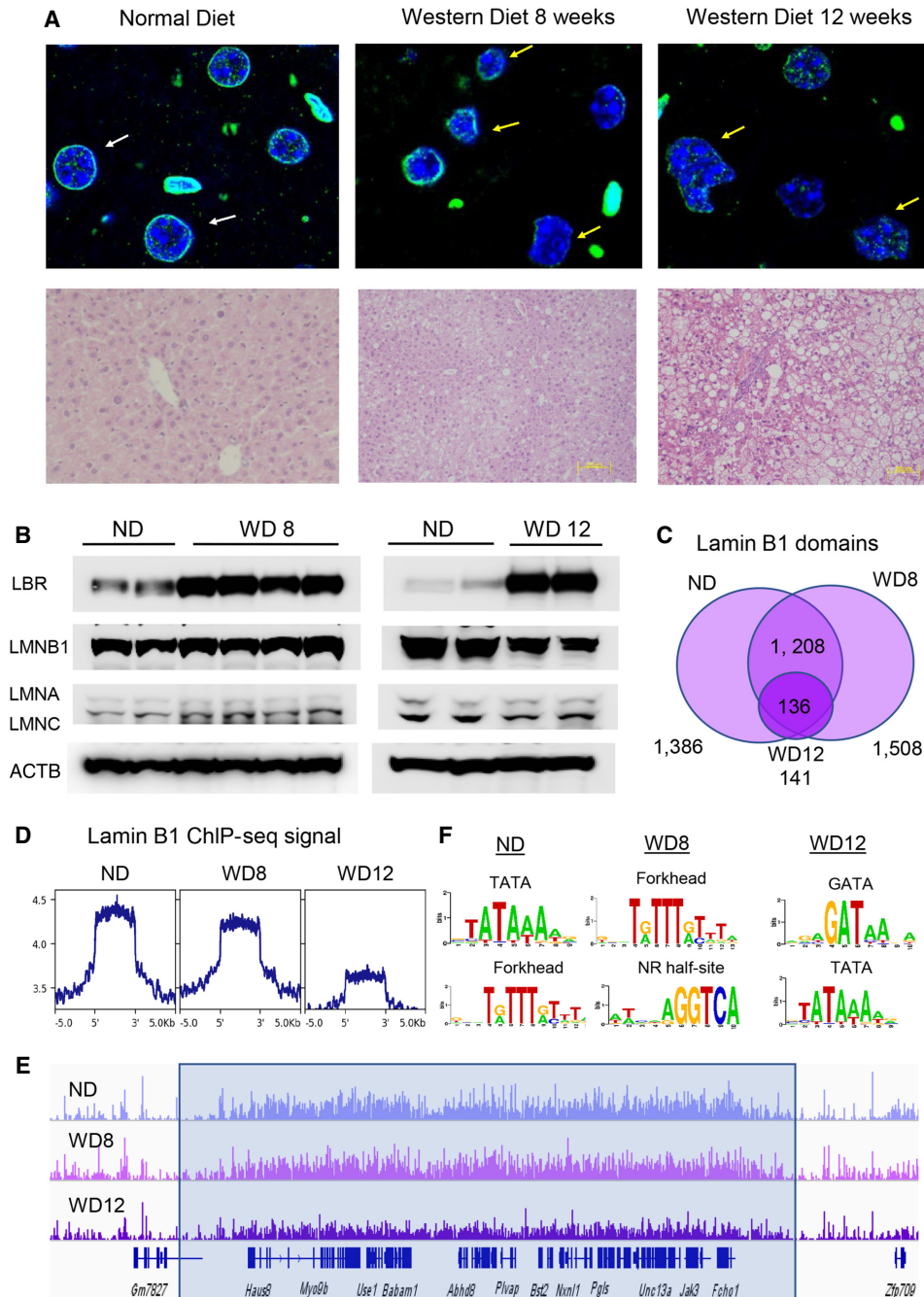


**Figure 2.** Nuclear lamina changes in diet-induced fatty liver. (A) Nuclear immunofluorescence (lamin B1; green) and DAPI nuclear staining of FFPE liver sections from mice on normal diet (ND; *top left*), WD8 (*top middle*), and WD12 (*top right*). Nuclei in mice on ND have a round shape (white arrows), whereas nuclei in mice on WD are irregular in shape and distorted (yellow arrows). Representative liver sections from ND and WD mice stained with H&E (*bottom*). Lipid accumulation is apparent on histological sections by the presence of lipid droplets in livers of mice on WD at 12 wk. (B) Western blot analysis of protein nuclear extracts from two control livers (ND) and four livers from mice on WD8 (*left*) and two control livers (ND) and two livers from mice on WD12 (*right*) with antibodies to LBR, LMNB1, LMNA/LMNC, and ACTB (loading control). Protein expression of LBR is increased in WD8, whereas that of LMNA, LMNB1, and LMNC is not altered (*left*). Protein expression of LBR is increased and LMNB1 (lamin B1) decreased in WD12, whereas that of LMNA and LMNC is not changed (*right*). (C) Venn diagram showing the results of genome-wide location analysis for lamin B1 (ChIP-seq) in livers on ND, WD8, and WD12, identifying 1,396 domains in ND, 1,508 in WD8, and 141 in WD12 called bound in both young and old livers by SICER. The number of LADs is comparable in WD8 (1,396 ND vs. 1,508 WD8). The number of LADs is greatly reduced in WD12 (1,396 ND vs. 141 WD12). (D) Lamin B1 ChIP-seq signal (reads per kilobase, per million mapped reads [RPKM]) calculated at LADs decreases with WD progression. (E) ChIP-seq track view in the Integrative Genome Viewer (IGV) of a representative LAD showing decreased lamin B1 ChIP-seq signal for WD at 12 wk. (F) Scanning motif of positional weight matrices in the JASPAR and TRANSFAC databases in LADs in ND (*left*), WD8 (*middle*), and WD12 (*right*). PscanChIP identified highly enriched consensus sites for A/T-rich sequences, including TATA box ( $P$ -value  $< 8.9 \times 10^{-108}$ ) and the forkhead motif ( $P$ -value  $< 8.8 \times 10^{-93}$ ) in ND, forkhead consensus ( $P$ -value  $< 4.9 \times 10^{-106}$ ) and nuclear receptor half-site ( $P$ -value  $< 6.7 \times 10^{-32}$ ) in WD8, and GATA consensus ( $P$ -value  $< 1.4 \times 10^{-8}$ ) and A/T-rich TATA box motif ( $P$ -value  $< 1.8 \times 10^{-5}$ ) in WD12.

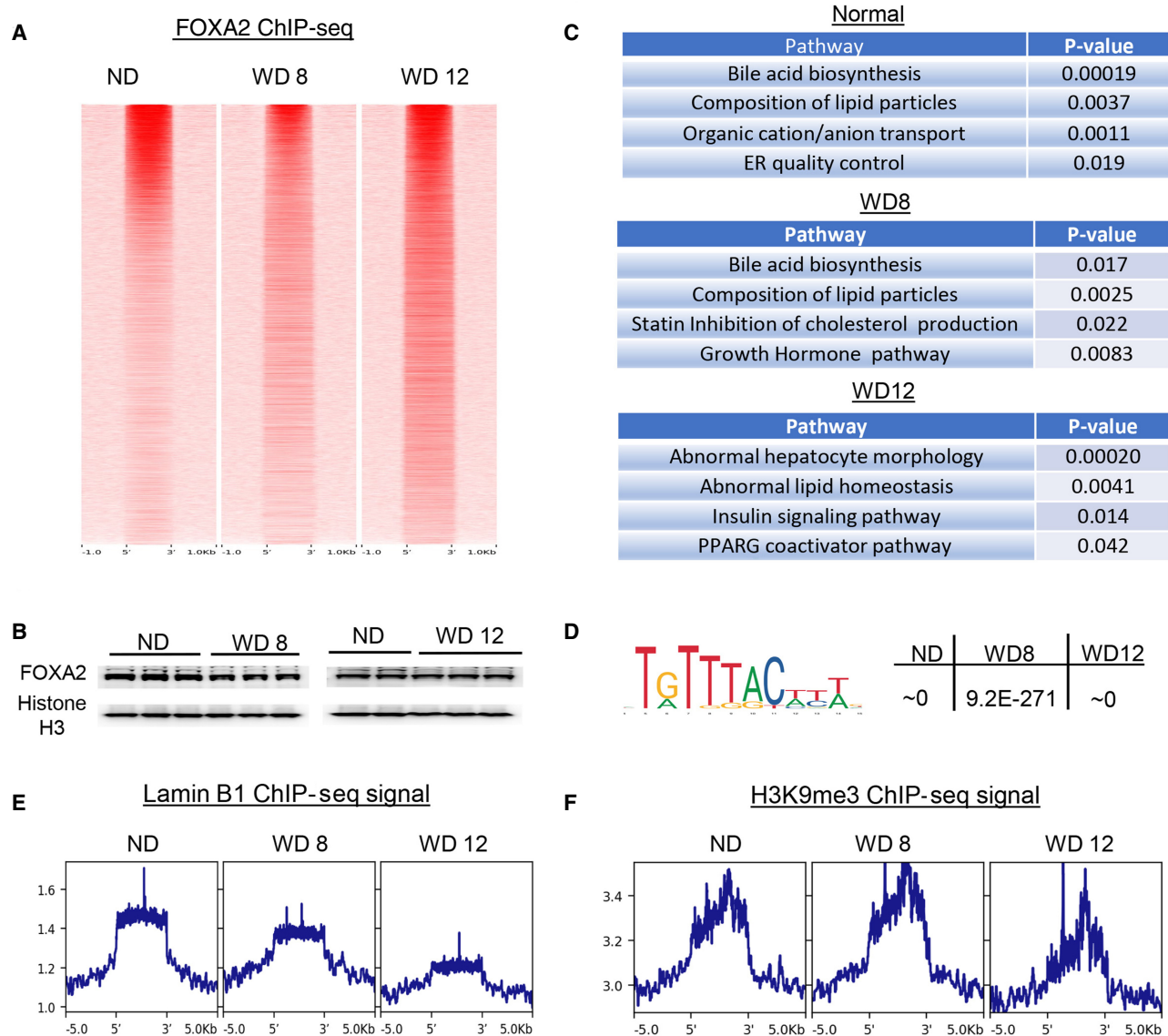


**Figure 3.** FOXA2 binding increases in diet-induced fatty liver. (A) Heatmap of results of FOXA2 ChIP-seq showing that binding increases in livers of mice on WD (6985 sites in ND, 12,765 in WD8, 9695 in WD12). (B) Western blot analysis of protein nuclear extracts from two control livers (ND) and three livers from mice on WD8 (left) and two control livers (ND) and three livers from mice on WD12 (right) with antibodies to FOXA2 and histone H3 (loading control). FOXA2 protein expression does not change in mice on WD8 and WD12; hence, changes in FOXA2 binding are independent of its expression. (C) Enrichr analysis of overrepresented pathways in sites bound by FOXA2 in ND, WD8, and WD12. (D) Scanning motif of positional weight matrices in the JASPAR and TRANSFAC databases in regions bound by FOXA2 in each condition by PscanChIP identified highly enriched forkhead consensus sites for FOXA2. (E) Lamin B1 ChIP-seq signal (RPKM) calculated in the overlap of lamin B1 domains in ND with FOXA2-binding sites in WD12 decreases with diet and steatosis progression. (F) H3K9me3 ChIP-seq signal (RPKM) calculated in the overlap of lamin B1 domains in ND with FOXA2-binding sites in WD12 decreases only at WD12.

lamina-associated protein in mouse liver leads to steatosis and steatohepatitis through aberrant growth hormone signaling (Kwan et al. 2017). Pathways consistent with the phenotype, including “abnormal hepatocyte morphology,” “abnormal lipid homeostasis,” and “ppar-gamma coactivator pathway,” were overrepresented in FOXA2-bound regions in WD12. The scanning motif of positional weight matrices in the JASPAR and TRANSFAC databases in regions bound by FOXA2 in each condition by PscanChIP (Zambelli et al. 2013) identified highly enriched forkhead consensus sites for FOXA2 (Fig. 3D).

Similar to our analysis in old livers (Whitton et al. 2018), we compared increased FOXA2 binding to changes in lamin B1 occu-

pancy. We computed the overlap of all lamin B1 domains in ND with FOXA2-binding sites in WD12 and found 826 such domains. An average profile of lamin B1 occupancy at these sites in ND, WD8, and WD12 is shown in Figure 3E. Lamin B1 signal is considerably reduced at these regions with progression of the diet and steatosis. We performed a similar analysis of heterochromatin content using H3K9me3 ChIP-seq and show that a decrease in heterochromatin mark is observed only in WD12 when altered FOXA2 binding is influenced by changes at the lamina (Supplemental Fig. S1; Fig. 3F). Hence, the pioneering activity of FOXA2 at WD12 correlates with opening of chromatin and derepression of genes previously located in lamina domains.

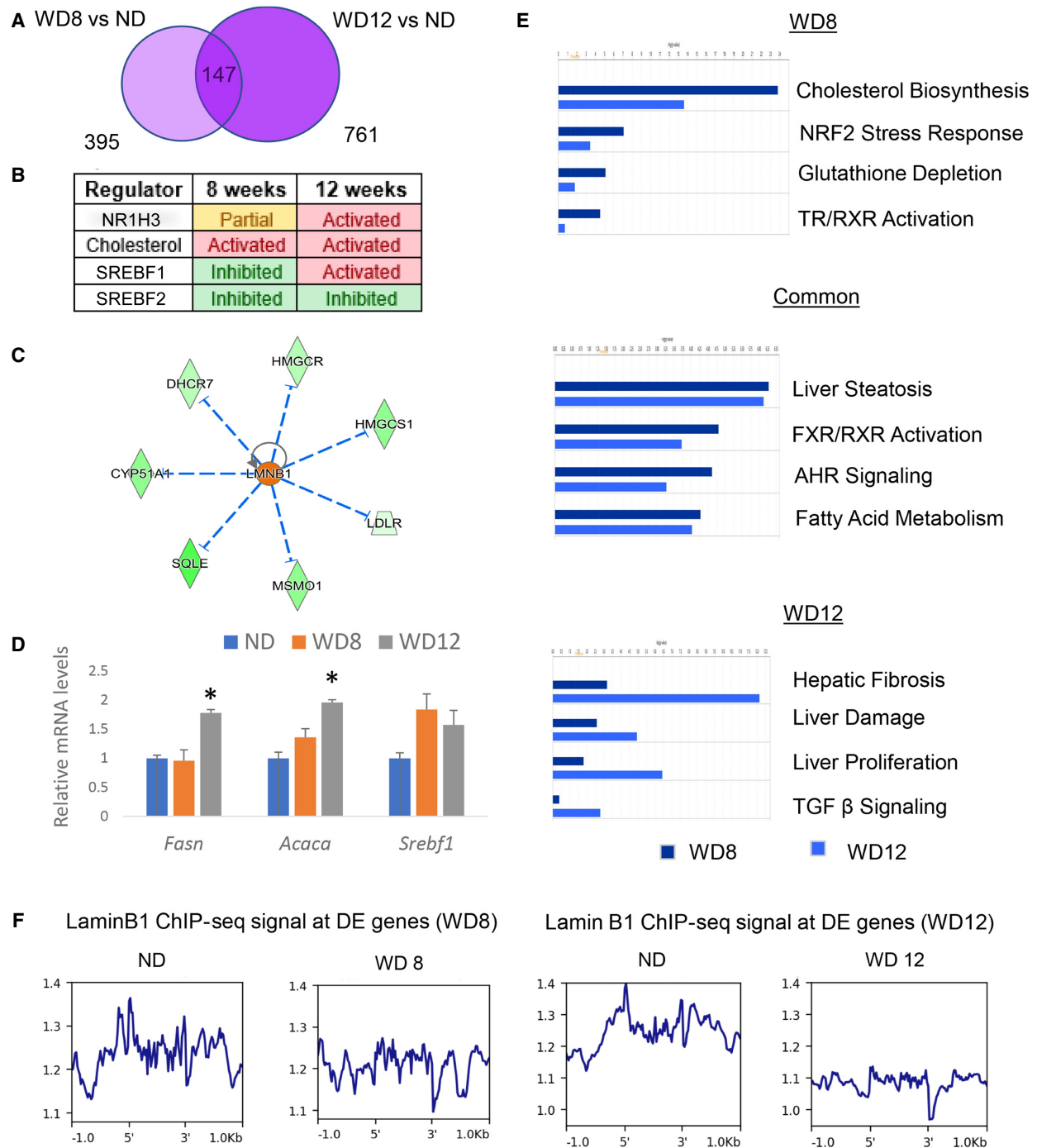


**Figure 4.** Differential expression analysis of genes on WD. (A) Venn diagram showing that the expression of 395 genes changes at WD8, whereas the mRNA levels of 761 transcripts were altered at WD12 (overlap of 147 genes). (B) Ingenuity pathway analysis (IPA) of differential gene expression identified multiple upstream regulators. Genes activated by the presence of cholesterol were activated, whereas cholesterol synthesis and other enzymes regulated by SREBF2 were repressed in a negative feedback loop in both WD8 and WD12. Despite increased transcription of cholesterol-regulated genes, activity of NR1H3, activated by binding of oxysterol, a derivative of cholesterol, is only partially activated in WD8. Changes at the nuclear lamina associated with derepression of additional NR1H3 targets lead to full activation of LXR-dependent gene expression in WD12. Although cholesterol controls gene expression in WD8 and WD12 in the same direction, the activity of SREBF1 is repressed in WD8 but activated in WD12. (C) IPA also identified a network relating increased activity of lamin B1 (LMNB1) with reduced expression of cholesterol-synthesizing enzymes in WD8. (D) mRNA levels of *Fasn* and *Acaca* genes, SREBF1 targets crucial for lipogenesis, by quantitative RT-PCR. Expression of *Fasn* and *Acaca* does not change in livers of mice on WD8 but significantly increases in livers of mice on WD12, correlating to phenotypic changes (severe steatosis at WD12). (\*)  $P$ -value  $< 0.05$ . (E) Pathways identified by IPA analysis of differential gene expression include “cholesterol biosynthesis” and “NRF2 stress response,” which are enriched in WD8, and “liver steatosis” and “FXR/RXR activation,” which are equally significant in both conditions. “Hepatic fibrosis,” “TGF  $\beta$  signaling,” and “liver damage” are highly enriched at WD12 before the fibrosis phenotype. (F) Lamin B1 ChIP-seq signal (RPKM) calculated at loci with gene expression changes in WD8 (left) and WD12 (right) is reduced in both conditions; hence, changes at the nuclear lamina are directly linked to altered gene expression in WD.

## Changes at the nuclear lamina are linked to altered gene expression in WD

We also performed RNA-seq in livers of mice on ND and WD and determined that the expression of 395 genes changes at WD8, whereas the mRNA levels of 761 of transcripts were altered at WD12 (Fig. 4A). Ingenuity pathway analysis (IPA) of differential gene expression identified multiple upstream regulators listed in Figure 4B. Genes activated by the presence of cholesterol were activated, whereas cholesterol synthesis and other enzymes regulated by SREBF2 were repressed in a negative feedback loop (Brown and Goldstein 1997) in both in WD8 and WD12. IPA also identified a network relating increased activity of lamin B1 (LMNB1) with reduced expression of cholesterol-synthesizing enzymes (Fig. 4C) in WD8. The analysis is based on a previous study reporting that overexpression of lamin B1 in oligodendrocytes leads to decreased levels of genes in the cholesterol synthesis pathway (Rolyan et al. 2015). Although the expression of lamin B1 is not changed, protein levels of its receptor, LBR, are increased at WD8. It is possible that the increased activity of lamin B1 predicted by IPA analysis is correlated to induction of lamin B receptor (LBR) expression.

Despite increased transcription of cholesterol-regulated genes (Fig. 4B), activity of NR1H3, activated by binding of oxysterol, a derivative of cholesterol, is only partially activated in WD8 (Fig. 4B; Supplemental Fig. S2, top left). Changes at the nuclear lamina associated with derepression of additional NR1H3 targets (Fig. 1) leads to full activation of NR1H3-dependent gene expression in WD12 (Fig. 4B; Supplemental Fig. S2, top right). We also observe full activation of PPARA-dependent gene expression with a network of 66 genes at WD12 (Supplemental Fig. S2, bottom). Although cholesterol controls gene expression in WD8 and WD12 in the same direction, the activity of SREBF1 is repressed in WD8 but activated in WD12 (Fig. 4B). Lipogenesis is a critical pathway regulated by the SREBF1 targets *Fasn* and *Acaca*. Although the expression of both is not changed in WD8, mRNA levels of these genes are significantly increased in WD12 (Fig. 4D), contributing to the observed fatty liver phenotype.

Pathways identified by IPA analysis of differential gene expression included “cholesterol biosynthesis” and “NRF2 stress response,” which were enriched in WD8, and “liver steatosis” and “FXR/RXR activation,” which were equally significant in both conditions. “Hepatic fibrosis,” “TGF  $\beta$  signaling,” and “liver damage” were highly enriched at WD12 before the fibrosis phenotype (Fig. 4E). Lastly, we investigated whether lamin B1 occupancy changes at loci of differentially expressed genes in WD. Lamin B1 ChIP-seq signal is reduced for genes with expression changes in both WD8 (Fig. 4F, left) and WD12 (Fig. 4F, right). Hence, changes at the nuclear lamina are directly linked to altered gene expression in WD.

## Nuclear lamina changes in NAFLD patients

Based on the results in the diet-induced mouse model, we proceeded to examine nuclear lamina changes in younger NAFLD patients (normal controls, mild steatosis, severe steatosis; healthy, 26–45 yr old; NAFLD, 21–51 yr old) (for study design, see Fig. 1). Indeed, the nuclear shape in NAFLD patients with mild or severe steatosis was altered (Fig. 5A). The circularity of nuclei is significantly changed in NAFLD patients with both mild and severe steatosis (Supplemental Fig. S1). In addition, the protein expression of the lamina-associated proteins LBR and lamin A (LMNA) is increased in most patients with NAFLD. Protein levels of lamin B1 (LMNB1) are decreased in some NAFLD patients (Fig. 5B). We performed lamin B1 ChIP-seq in human patients and found a similar

number of domains in control and NAFLD patients (1345 in normal, 1457 in mild steatosis, and 1616 in severe steatosis). About a third of lamin B1-associated regions are bound exclusively in each condition (Fig. 5C), similar to the changes we reported in an aged mouse model of fatty liver (Whitton et al. 2018). The lamin B1 ChIP-seq signal decreases significantly in NAFLD patients, to the same extent in mild and severe steatosis (Fig. 5D). PscanChIP identified highly enriched consensus sites for the forkhead motif in all patients (Fig. 5E).

## FOXA2 binding is redistributed in NAFLD patients

Next, we assessed FOXA2 occupancy and found that it is redistributed in NAFLD livers (6623 regions in normal, 4578 regions in mild steatosis, 9964 regions in severe steatosis) (Fig. 6A; for heatmap of FOXA2 binding in each patient, see Supplemental Fig. S3). PscanChIP motif analysis (Zambelli et al. 2013) identified highly enriched forkhead consensus sites for FOXA2 in all conditions (Fig. 6B). FOXA2 binding does not change in patients with mild steatosis and is redistributed and increases in patients with severe steatosis despite a reduction in FOXA2 protein levels (Fig. 6C). Similar to the analysis in the mouse model (Fig. 3E), we computed an overlap of all lamin B1 domains in normal patients with FOXA2 binding sites in patients with severe steatosis and found 1029 such domains. Lamin B1 signal is considerably reduced at these regions in NAFLD patients to the same extent in mild and severe steatosis (Fig. 6D). We have previously shown FOXA2 expression is reduced in human patients with cholestatic livers (subjects with biliary atresia [BA] and primary sclerosing cholangitis [PSC]) (Bochkis et al. 2008). In addition, ligand activation of NR1H4 and NR1H3 increases FOXA2 binding three- to fivefold without changes in the FOXA2 protein levels (Kain et al. 2021). Hence, a reduction in FOXA2 expression in NAFLD is similar to changes observed in cholestasis. Additional FOXA2 binding is likely owing to untethering of heterochromatin owing to lamina shape changes (Fig. 5A) and reduction of lamin B1 signal at all LADs (Fig. 5D) and LADs with additional FOXA2 binding in NAFLD (Fig. 6D). Although LADs are redistributed and lamin B1 ChIP-seq signal decreases significantly in NAFLD patients, to the same extent in mild and severe steatosis, FOXA2 binding is repositioned only in patients with more severe steatosis. Hence, changes at the nuclear lamina reshape FOXA2 binding with progression of the disease.

Next, we mapped FOXA2 bound regions to closest genes using GREAT (McLean et al. 2010) and selected 1000 genes that mapped closest to the TSS for pathway analysis with Enrichr. Overrepresented pathways included “bile acid and bile salt biosynthesis,” “FOXA2 pathway,” and “nuclear receptors in lipid metabolism” for FOXA2 sites in normal patients. Pathways consistent with the phenotype, including “oxysterol pathway,” “PPAR pathway,” and “telomere attrition/genomic instability,” were overrepresented in FOXA2-bound regions in NAFLD livers (Fig. 6E). Overall, changes at the nuclear lamina observed in a diet-induced mouse model of fatty liver in young mice and the mechanism relating chromatin regulation and binding of pioneer factors are corroborated in younger human patients.

## A model relating chromatin regulation at the nuclear lamina and binding of pioneer factors in NAFLD

Our results in a diet-induced mouse model of fatty liver and NAFLD patients led to a model relating chromatin regulation at the nuclear lamina and binding of pioneer factors. In healthy conditions, repressed heterochromatin regions that should not be

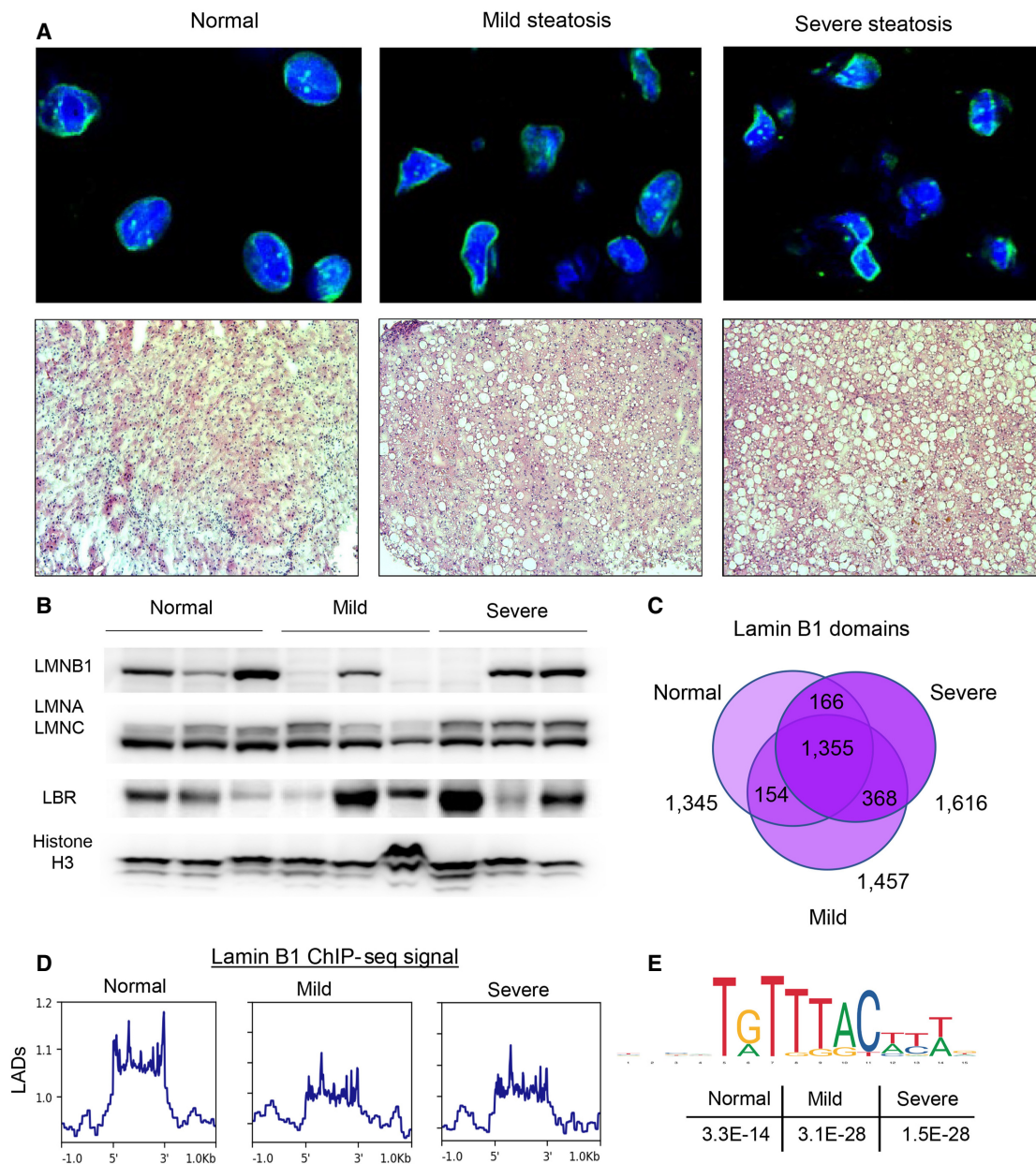


**Figure 5.** Nuclear lamina changes in patients with NAFLD. (A) Nuclear immunofluorescence (lamin B1; green) and DAPI nuclear staining of frozen liver sections from patients with normal (top left) and fatty livers (top middle and right). Nuclei in individuals with normal livers have a round shape, whereas nuclei in NAFLD patients are irregular in shape and distorted. (Bottom) Representative liver sections from normal and NAFLD patients stained with H&E. Lipid accumulation is apparent on histological sections by presence of lipid droplets in NAFLD livers. (B) Western blot analysis of protein nuclear extracts from livers of three normal and six NAFLD patients with antibodies to LBR, LMNB1, LMNA/LMNC, and Histone H3 (loading control). Protein expression of LBR and lamina A (LMNA) is increased in most patients with NAFLD. Protein levels of lamin B1 (LMNB1) are decreased in some NAFLD patients. (C) Venn diagram showing the results of genome-wide location analysis for lamin B1 (ChIP-seq) in livers of normal and NAFLD patients, identifying 1345 domains in normal, 1457 in mild steatosis, and 1616 in severe steatosis, of which 1355 were called bound in all conditions by Epic. (D) Lamin B1 ChIP-seq signal (RPKM) calculated at LADs decreases significantly in NAFLD patients to the same extent in mild and severe steatosis. (E) PscanChIP identified highly enriched consensus sites for the forkhead motif in all patients.

expressed in hepatocytes are sequestered to the lamina (Fig. 7A). Changes at the lamina, owing to either a genetic mutation or environment (diet), lead to untethering of heterochromatin (Fig. 7B) and subsequent recruitment of pioneer factor FOXA2 to previously repressed regions (Fig. 7C). Binding of FOXA2 opens chromatin for additional factors, leading to derepression of gene expression regulating lipid synthesis and storage and resulting in

steatosis (Fig. 7D). We have previously reported this mechanism in aged mouse and genetic laminopathy models. Genetic laminopathies cause a fatty liver phenotype and changes in heterochromatin that are completely reproduced in aging liver (Whitton et al. 2018). In this study, we show that a similar mechanism leads to steatosis irrespective of aging in both young mice placed on WD and younger NAFLD patients.

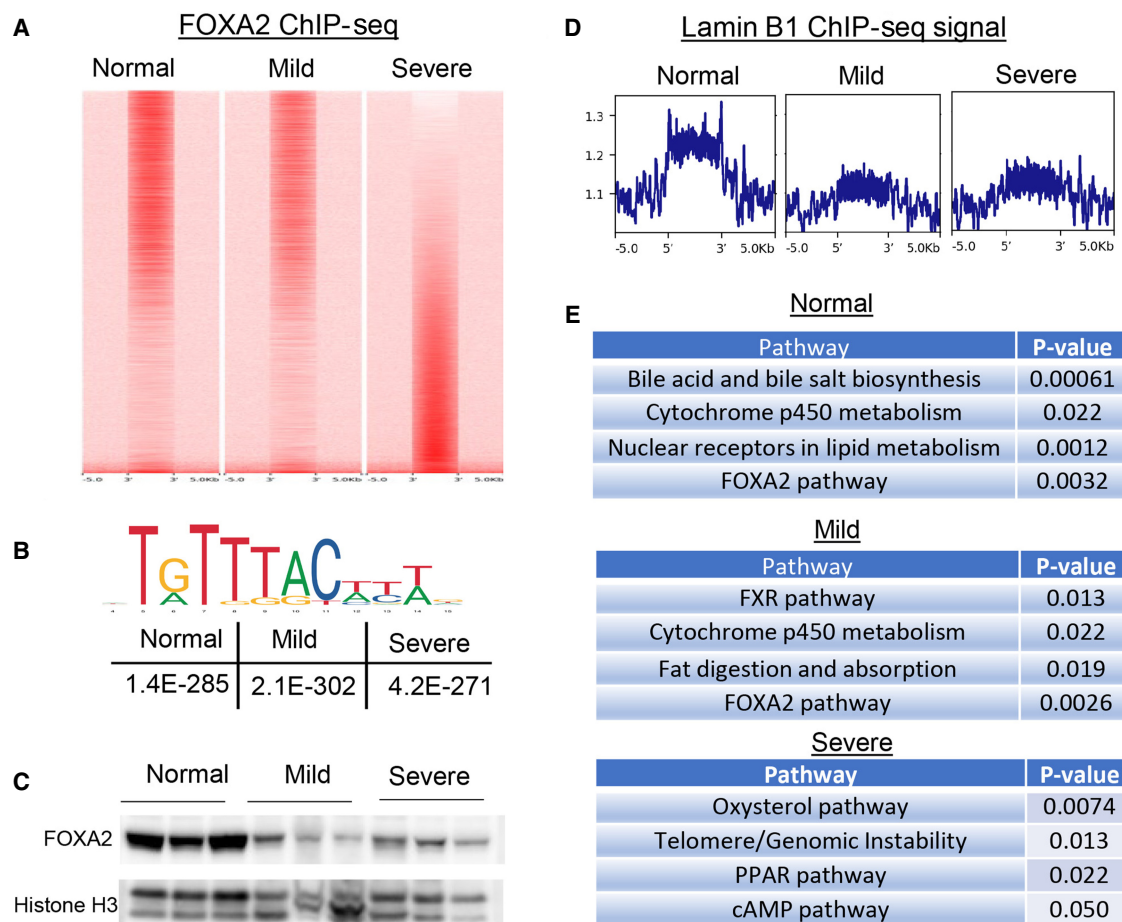


**Figure 6.** FOXA2 binding is redistributed in NAFLD patients. (A) Heatmap of results of FOXA2 ChIP-seq showing that binding increases in livers of mice on WD (6623 sites in normal, 4578 in mild steatosis, 9664 in NAFLD). (B) PscanChIP motif analysis identified highly enriched forkhead consensus sites for FOXA2 in both conditions. (C) Western blot analysis of protein nuclear extracts from the livers of three normal and six NAFLD patients with antibodies to FOXA2 and histone H3 (loading control). FOXA2 protein levels decrease in NAFLD patients. (D) Lamin B1 ChIP-seq signal (RPKM) calculated in the overlap of lamin B1 domains in normal patients with FOXA2-binding sites in NAFLD patients with severe steatosis is considerably reduced in NAFLD patients to the same extent in mild and severe steatosis. (E) Enrichr analysis identified overrepresented pathways “bile acid and bile salt biosynthesis,” “FOXA2 pathway,” and “nuclear receptors in lipid metabolism” for FOXA2 sites in normal patients. Pathways consistent with the phenotype, including “oxysterol pathway,” “PPAR pathway,” and “telomere attrition/genomic instability,” were overrepresented in FOXA2-bound regions in NAFLD livers.

## Discussion

Our previous study in aging liver underscored the importance of examining how dysregulation of heterochromatin at the nuclear lamina results in metabolic dysfunction (Whitton et al. 2018). Several studies have reported changes at the nuclear lamina in patients with metabolic disease and NAFLD. Genetic variants in the nuclear lamina-related genes *ZMPSTE24* and *TMPO*, which encode LAP2, and changes in nuclear morphology parameters have been observed in NAFLD patients (Brady et al. 2018; Segovia-Miranda et al. 2019). In addition, a high incidence of laminopathy was found among patients with metabolic syndrome (Dutour et al. 2011). Cells from these individuals presented with a dysmorphic nuclear shape and abnormal nuclear distribution of lamin A. These patients, in addition to being younger, also had hypertriglyceridemia and elevated ALT levels compared with other metabolic syndrome patients, suggesting liver dysfunction. Furthermore, a heterozygous mutation in *ZMPSTE24* was found in a patient with severe metabolic syndrome (Galant et al. 2016).

Fibroblasts from this individual showed nuclear shape abnormalities, and the patient presented with early onset T2D, liver steatosis, and hypertriglyceridemia. Collectively, these observations support the hypothesis that changes at the nuclear lamina promote hepatic fat accumulation in humans.

In this study, we show that changes in nuclear morphology alter LAD partitioning (LADs profiled by lamin B1 ChIP-seq) and reduced lamin B1 signal correlate with increased FOXA2 binding before severe steatosis in young mice placed on WD. These alterations precede severe triglyceride accumulation and activation of enzymes crucial for lipogenesis. We also show that the nuclear shape and expression of several lamina-associated proteins are changed in NAFLD patients with varying degrees of steatosis. In addition, LADs are redistributed and lamin B1 ChIP-seq signal decreases significantly in younger NAFLD patients to the same extent in mild and severe steatosis. In contrast, FOXA2 binding is similar in normal and NAFLD patients with moderate steatosis and is repositioned only in NAFLD patients with more severe lipid accumulation. Hence, changes at the nuclear lamina reshape FOXA2

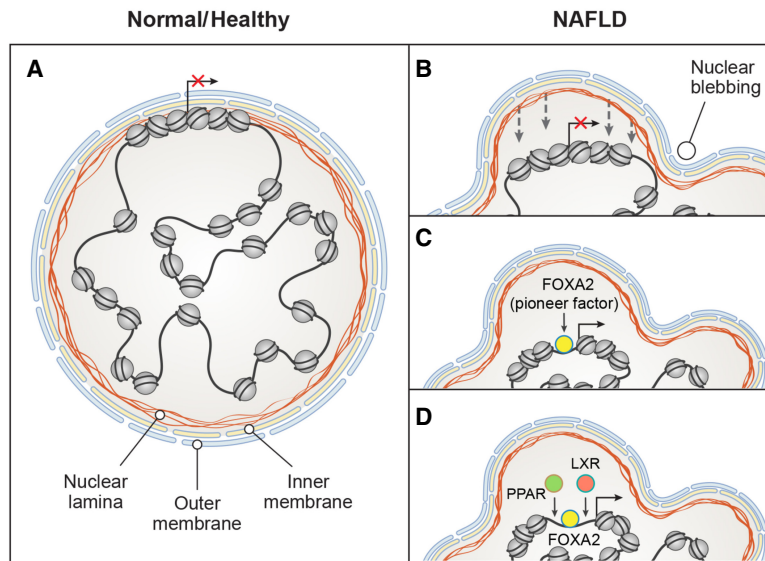


**Figure 7.** A model relating chromatin regulation at the nuclear lamina and binding of pioneer factors in NAFLD. (A) In normal healthy conditions, repressed regions that should not be expressed in a given tissue are sequestered and tethered to the nuclear lamina. (B) Disturbance in nuclear architecture, either owing to a genetic mutation or environment (diet), leads to portions of heterochromatin to detach from the nuclear lamina, as well as destabilization of the nuclear membrane and nuclear blebbing. (C) Condensed heterochromatin that is no longer attached to the nuclear lamina can be bound by pioneer factors such as FOXA2. Sequences associated with the lamina as well as forkhead binding motifs are A/T-rich. (D) Binding of FOXA2 opens previously repressed chromatin, facilitating recruitment of additional factors, such as PPAR and LXR, and activation (or derepression) of gene expression. We observe activation of LXR- and PPAR-dependent gene expression in livers of mice on WD. Also, LXR and PPAR pathways are enriched at loci bound by redistributed FOXA2 in NAFLD patients.

binding with progression of the disease. Overall, changes at the nuclear lamina observed in the diet-induced mouse model of fatty liver and the mechanism relating chromatin regulation and binding of pioneer factors are corroborated in human patients. Our results suggest a role for nuclear lamina in the etiology of NAFLD irrespective of aging, possibly leading to improved stratification of patients and novel treatments aimed at restoring nuclear lamina function.

We observe changes in expression of several lamina-associated proteins, LBR, lamin A, and lamin B1, in both mice with fatty liver and NAFLD patients. In mice, the activation of LBR precedes severe triglyceride accumulation, and reduction in lamin B1 expression is detected later. Reducing LBR up-regulation or restoring lamin B1 expression in the diet-induced fatty liver could reestablish proper nuclear shape and reduce triglyceride accumulation and warrants further study. In addition, it is not clear why expression of these proteins changes in the mouse model of fatty liver and NAFLD patients. One explanation could be that metabolic changes during the progression of the disease produce ligands for nuclear receptors, such as LXR and PPAR, and activate ligand-dependent gene expression, including *Lbr*, *Lmna*, and *Lmnb1*.

We have confirmed the relationship between changes at the lamina and binding of pioneer factors, first reported in an aging liver and laminopathy model, in younger NAFLD patients. Lamina shape changes and LAD redistribution before severe triglyceride accumulation in mice correlate with increased FOXA2 binding, whereas FOXA2 expression is not changed in a mouse model of NAFLD. In contrast, although LADs are repartitioned in NAFLD patients with both mild and severe steatosis, FOXA2 binding, despite reduced expression, is reshaped only in individuals with severe

steatosis. Hence, changes at the nuclear lamina reshape FOXA2 binding with progression of the disease. Although the expression of FOXA2 is regulated differently in mice and humans, likely affecting timing of binding changes, the pioneer factor plays the same role in both settings. We previously showed that FOXA2 is required to open chromatin for ligand activation of nuclear receptors (Kain et al. 2021). FOXA2 binding is increased and redistributed in NAFLD patients, allowing for recruitment of nuclear receptors to these newly opened sites. Restricting FOXA2 binding to proper loci, occupied only in healthy liver, is key in halting the progression of the disease. Restoring the lamina shape will preserve its function by tethering the heterochromatin and preventing FOXA2 from accessing those regions.

No specific cause of NAFLD has been established, and currently, there is no approved treatment for the disease. We propose a novel mechanism relating changes at the nuclear lamina that alter binding of a pioneer factor, leading to opening of previously repressed chromatin and up-regulation of lipid synthesis and storage pathways to development of steatosis in NAFLD (Fig. 7). We hypothesize that maintaining the nuclear

lamina function and keeping the nucleus and the genome intact will keep the organism healthy. Then, the cell will be able to maintain integrity of the genome by preserving DNA in its proper configuration to activate and repress gene expression appropriate for each cell type. Hence, treating NAFLD as a laminopathy and testing approaches to restore the nuclear lamina shape and function in a diseased state could lead to reversal of the phenotype.

## Methods

### Animals

We used a diet-induced mouse model of NAFLD for our studies (Asgharpour et al. 2016). Eight- to 12-wk-old heterozygous C57BL/6J (B6)/129S1/SvImJ (S129) mice were fed WD (42% kcal from fat and containing 0.1% cholesterol; Harlan TD.88137) with ad libitum consumption of glucose and fructose (SW; 23.1 g/L d-fructose +18.9 g/L d-glucose) (Asgharpour et al. 2016) for 8–12 wk.

### Human studies

Liver tissue samples from donors (three healthy, three NAFLD with mild steatosis, and three NAFLD with severe steatosis) were obtained from the Sekisui XenoTech Biobank. Donors were 21–51 yr old (healthy, 26–45; NAFLD, 21–51).

### Immunofluorescence and immunohistochemistry

Frozen sections were fixed with precooled acetone:100%EtOH (1:1) for 10 min and subsequently washed with 1× PBS (5 min × three). Fresh liver tissue was fixed in 4% PFA overnight at 4°C

and embedded in paraffin as previously described (Zhang et al. 2005). Indirect immunofluorescence (lamin B1, Abcam Ab16048, 1:1000) and immunohistochemistry were performed as previously described (Zhang et al. 2005). Slides subject to immunohistochemistry were counterstained with H&E. DAPI DNA fluorescent stain (Sigma-Aldrich; 1 µg/mL) was used to detect nuclei.

### Chromatin immunoprecipitation and ChIP-seq

Snap-frozen mouse or human liver (100 mg) was used to prepare chromatin. ChIP and ChIP-seq were performed as reported previously (Kain et al. 2021). Briefly, liver tissue was minced in cold PBS and cross-linked in 1% formaldehyde/PBS for 15 min with constant rotation in a Labquake tube rotator. Cross-linking was quenched by adding glycine to a final concentration of 0.125 M. Nuclear lysate was sonicated using a Diagenode Bioruptor Pico for 14 cycles (30 sec on/30 sec off). FOXA2-specific rabbit antiserum (Seven Hills Bioreagents WRAB-1200), rabbit antibody to lamin B1 (Abcam Ab16048), and anti-Histone H3 (trimethyl K9) rabbit antibody (ab8898) were used for immunoprecipitation. Libraries were made according to standard Illumina protocol (end-repair of ChIP DNA, addition of A base to the 3'-ends, adapter ligation, and amplification). We used multiplex adapters for sequencing and Kapa HiFi DNA polymerase (Kapa Biosystems) for PCR amplification (16 cycles). Library fragments were isolated using Pippin Prep agarose gel. The purified DNA was captured on an Illumina flow cell for cluster generation. Libraries were sequenced on Illumina NextSeq 500 and NextSeq 2000 instruments following the manufacturer's protocols.

### RNA isolation, analysis, and sequencing

Liver RNA was isolated from heterozygous C57BL/6J (B6)/129S1/SvImJ (S129) mice fed either control or WD as described previously (Kain et al. 2021). The quality of the RNA samples was analyzed using an Agilent RNA 6000 nano kit (Bioanalyzer, Agilent Technologies). Samples with RIN scores above 9.5 were used in library preparation. One microgram of total RNA was used to isolate mRNA (NEBNext Poly(A) mRNA magnetic isolation module). Libraries of the resulting mRNA were prepared using a NEBNext Ultra II RNA library preparation kit. All samples were sequenced on an Illumina NextSeq 500. Four replicates were sequenced for ND and WD8; three replicates, for WD12. Analysis of mRNA expression levels for these samples was performed as described previously (Whitton et al. 2018). *Gapdh* was used as normalizing gene for quantitative RT-PCR analysis. Primer sequences are provided in Supplemental Table S1. Lists of differentially expressed genes for WD8 and WD12 are provided in Supplemental Table S2.

### Protein analysis

Protein extracts preparation and protein immunoblot analysis were performed as reported previously (Bochkis et al. 2008). The primary antibodies used were rabbit antibody to FOXA2 (Seven Hills Bioreagents WRAB-1200, 1:1000), rabbit antibody to histone H3 (Cell Signaling 4499, 1:4000), mouse antibody to LAMIN A/C (Cell Signaling mAb 4777, 1:2000), rabbit antibody to LAMIN B (Abcam ab16048, 1:1000), mouse antibody to LBR (Millipore MABT831, 1:1.000), and mouse antibody to ACTB (Sigma-Aldrich A3854, 1:5000).

### ChIP-seq analysis

Reads were aligned to the mouse genome (mm10; NCBI Build 38) and human genome (hg19; NCBI build 37) using BWA v0.7.12 (Li and Durbin 2009). Duplicate reads were removed using Picard v

1.134 (<http://picard.sourceforge.net>). Reads (Phred score  $\geq 30$ ) that aligned uniquely were used for subsequent analysis. Data from two murine biological replicates were merged for FOXA2, lamin B1, and H3K9me3 ChIP-seq comparison (two ND, two WD8, two WD12). Data from three human patients were merged for FOXA2 and lamin B1 binding (three normal and three NAFLD). LADs in mouse lamin B1 ChIP-seq were determined by SICER (mm10 as species, window size 10,000 bp, gap size 10,000 bp, FDR 10%) (Xu et al. 2014). Using hg19 (GRCh37) as opposed to the GRCh38 build would not significantly change the conclusions because a very strong forkhead motif was detected in FOXA2 ChIP-seq, and significant A/T-rich motifs were identified in lamin B1 ChIP-seq, as expected. Epic peak caller (Xu et al. 2014; <https://github.com/biocore-ntnu/epic2>) was used to determine lamin B1-associated domains in human patients (hg19 as species, window size of 10 kb, gap size of three, FDR 5%). PeakSeq (Rozowsky et al. 2009) was used to identify FOXA2 bound peaks against input controls (mouse: FDR 5%,  $Q$ -value  $< 1.5 \times 10^{-2}$ ; human: FDR 5%,  $Q$ -value  $< 0.07$ ).

### RNA-seq analysis

RNA-seq reads were aligned using STAR (Dobin et al. 2013) to mouse genome build mm10. Expression levels were calculated using RSEM (Li and Dewey 2011). Differential expression analysis of RNA-seq ( $P$ -value  $< 0.05$ ) was performed in R using edgeR package (Robinson et al. 2010) with a Benjamini-Hochberg FDR of 5%. Four replicates were sequenced for ND and WD8; three replicates, for WD12.

### Functional analysis

Sequencing reads were visualized with the Integrative Genome Viewer (IGV) (Robinson et al. 2011). Heatmaps of ChIP-seq coverage were generated by deepTools (Ramírez et al. 2014). The overlap between different categories of binding sites was computed using Galaxy genome analysis tools (Hillman-Jackson et al. 2012). Sequence analysis for overrepresented transcription factor binding motifs in regions from ChIP-seq experiments was performed by PscanChIP (Zambelli et al. 2013). ChIP-seq peaks were associated with closest genes using GREAT (McLean et al. 2010), which were subsequently used for pathway analysis with Enrichr (Kuleshov et al. 2016). IPA was used for pathway and network analysis of differentially expressed genes.

### Image quantification

Images were analyzed with the open-source CellProfiler software package. This software uses an automated algorithm to identify and measure nuclear morphology. This algorithm first loads images of DAPI-stained nuclei. Gaps in circular objects are filled to better preserve disk shapes. All images are background-subtracted based on object intensity. Distinct objects are then identified and segmented using an Otsu threshold of the DAPI image. A smoothing filter is applied to eliminate artifacts around the edges of the nuclei. Finally, the area and perimeter of these nuclei are measured and used to calculate circularity, which we defined by the following equation:

$$\text{Circularity} = \frac{4\pi * \text{area}}{\text{perimeter}^2}.$$

### Statistics

LADs in mouse lamin B1 ChIP-seq were determined by SICER (FDR 10%). Epic peak caller was used to determine lamin B1-associated

domains in human patients (FDR 5%). PeakSeq was used to identify FOXA2 bound peaks against input controls (mouse: FDR 5%,  $Q$ -value  $< 1.05 \times 10^{-2}$ ; human: FDR 5%,  $Q$ -value  $< 0.07$ ). Differential expression analysis of RNA-seq ( $P$ -value  $< 0.05$ ) was performed in R (R Core Team 2022) using edgeR package with a Benjamini–Hochberg FDR of 5%. Fisher's exact test was used by both IPA and Enrichr for overrepresented pathway analysis. A Student's two-sample  $t$ -test was used to analyze the Q-PCR data.

## Data access

All raw and processed sequencing data generated in this study have been submitted to the NCBI Gene Expression Omnibus (GEO; <https://www.ncbi.nlm.nih.gov/geo/>) under accession number GSE197399.

## Competing interest statement

The authors declare no competing interests.

## Acknowledgments

We thank L. Berk and M. Thakore for technical assistance. We thank M. Lazar for critical reading of the manuscript. I.M.B. is supported by National Institute of Diabetes and Digestive and Kidney Diseases R01 award DK121059.

**Author contributions:** Investigation, visualization, review, and editing were by X.W. Software, formal analysis, data curation, visualization, and review and editing were by M.A.M. Investigation, visualization, and review and editing were by Y.H. Software, formal analysis, data curation, visualization, and review and editing were by N.A.R. Software, formal analysis, and review and editing were by T.G.E. Conceptualization, supervision, and review and editing were by J.J.S. Conceptualization, formal analysis, investigation, writing the original draft, supervision, project administration, and funding acquisition were by I.M.B.

## References

- Asgharpour A, Cazanave SC, Pacana T, Seneshaw M, Vincent R, Banini BA, Kumar DP, Daita K, Min HK, Mirshahi F, et al. 2016. A diet-induced animal model of non-alcoholic fatty liver disease and hepatocellular cancer. *J Hepatol* **65**: 579–588. doi:10.1016/j.jhep.2016.05.005
- Bochkis IM, Rubins NE, White P, Furth EE, Friedman JR, Kaestner KH. 2008. Hepatocyte-specific ablation of *Foxa2* alters bile acid homeostasis and results in endoplasmic reticulum stress. *Nat Med* **14**: 828–836. doi:10.1038/nm.1853
- Bochkis IM, Schug J, Rubins NE, Chopra AR, O'Malley BW, Kaestner KH. 2009. Foxa2-dependent hepatic gene regulatory networks depend on physiological state. *Physiol Genomics* **38**: 186–195. doi:10.1152/physiolgenomics.90376.2008
- Bochkis IM, Schug J, Ye DZ, Kurinna S, Stratton SA, Barton MC, Kaestner KH. 2012. Genome-wide location analysis reveals distinct transcriptional circuitry by paralogous regulators Foxa1 and Foxa2. *PLoS Genet* **8**: e1002770. doi:10.1371/journal.pgen.1002770
- Brady GF, Kwan R, Ulintz PJ, Nguyen P, Bassirian S, Basrur V, Nesvizhskii AI, Looma R, Omary MB. 2018. Nuclear lamina genetic variants, including a truncated LAP2, in twins and siblings with nonalcoholic fatty liver disease. *Hepatology* **67**: 1710–1725. doi:10.1002/hep.29522
- Brown MS, Goldstein JL. 1997. The SREBP pathway: regulation of cholesterol metabolism by proteolysis of a membrane-bound transcription factor. *Cell* **89**: 331–340. doi:10.1016/S0092-8674(00)80213-5
- Dobin A, Davis CA, Schlesinger F, Drenkow J, Zaleski C, Jha S, Batut P, Chaisson M, Gingeras TR. 2013. STAR: ultrafast universal RNA-seq aligner. *Bioinformatics* **29**: 15–21. doi:10.1093/bioinformatics/bts635
- Dutour A, Roll P, Gaborit B, Courrier S, Alessi M-C, Tregouet D-A, Angelis F, Robaglia-Schlupp A, Lesavre N, Cau P, et al. 2011. High prevalence of laminopathies among patients with metabolic syndrome. *Hum Mol Genet* **20**: 3779–3786. doi:10.1093/hmg/ddr294
- Galant D, Gaborit B, Desgrouas C, Abdesselam I, Bernard M, Levy N, Merono F, Coirault C, Roll P, Lagarde A, et al. 2016. A heterozygous ZMPSTE24 mutation associated with severe metabolic syndrome, ectopic fat accumulation, and dilated cardiomyopathy. *Cells* **5**: 21. doi:10.3390/cells5020021
- Gan L, Chitturi S, Farrell GC. 2011. Mechanisms and implications of age-related changes in the liver: nonalcoholic fatty liver disease in the elderly. *Curr Gerontol Geriatr Res* **2011**: 831536. doi:10.1155/2011/831536
- Guelen L, Pagie L, Brasset E, Meuleman W, Faza MB, Talhout W, Eussen BH, de Klein A, Wessels L, de Laat W, et al. 2008. Domain organization of human chromosomes revealed by mapping of nuclear lamina interactions. *Nature* **453**: 948–951. doi:10.1038/nature06947
- Hillman-Jackson J, Clements D, Blankenberg D, Taylor J, Nekrutenko A. 2012. Using Galaxy to perform large-scale interactive data analyses. *Curr Protoc Bioinformatics* **Chapter 10**: Unit10.15. doi:10.1002/0471250953.bi100538
- Kain J, Wei X, Reddy NA, Price AJ, Woods C, Bochkis IM. 2021. Pioneer factor Foxa2 enables ligand-dependent activation of type II nuclear receptors FXR and LXR $\alpha$ . *Mol Metab* **53**: 101291. doi:10.1016/j.molmet.2021.101291
- Kuleshov MV, Jones MR, Rouillard AD, Fernandez NF, Duan Q, Wang Z, Koplev S, Jenkins SL, Jagodnik KM, Lachmann A, et al. 2016. Enrichr: a comprehensive gene set enrichment analysis web server 2016 update. *Nucleic Acids Res* **44**: W90–W97. doi:10.1093/nar/gkw377
- Kwan R, Brady GF, Brzozowski M, Weerasinghe SV, Martin H, Park MJ, Brunt MJ, Menon RK, Tong X, Yin L, et al. 2017. Hepatocyte-specific deletion of mouse lamin A/C leads to male-selective steatohepatitis. *Cell Mol Gastroenterol Hepatol* **4**: 365–383. doi:10.1016/j.jcmgh.2017.06.005
- Li B, Dewey CN. 2011. RSEM: accurate transcript quantification from RNA-Seq data with or without a reference genome. *BMC Bioinformatics* **12**: 323. doi:10.1186/1471-2105-12-323
- Li H, Durbin R. 2009. Fast and accurate short read alignment with Burrows–Wheeler transform. *Bioinformatics* **25**: 1754–1760. doi:10.1093/bioinformatics/btp324
- Mariño G, Ugalde AP, Salvador-Montoliu N, Varela J, Quirós PM, Cadiñanos J, van der Pluijm I, Freije JM, López-Otin C. 2008. Premature aging in mice activates a systemic metabolic response involving autophagy induction. *Hum Mol Genet* **17**: 2196–2211. doi:10.1093/hmg/ddn120
- McLean CY, Bristor D, Hiller M, Clarke SL, Schaar BT, Lowe CB, Wenger AM, Bejerano G. 2010. GREAT improves functional interpretation of cis-regulatory regions. *Nat Biotechnol* **28**: 495–501. doi:10.1038/nbt.1630
- Picard F, Géhin M, Annicotte J, Rocchi S, Champy MF, O'Malley BW, Chambon P, Auwerx J. 2002. SRC-1 and TIF2 control energy balance between white and brown adipose tissues. *Cell* **111**: 931–941. doi:10.1016/S0092-8674(02)01169-8
- Portillo-Sanchez P, Bril F, Maximov M, Lomonaco R, Biernacki D, Orsak B, Subbarayan S, Webb A, Hecht J, Cusi K. 2015. High prevalence of non-alcoholic fatty liver disease in patients with type 2 diabetes mellitus and normal plasma aminotransferase levels. *J Clin Endocrinol Metab* **100**: 2231–2238. doi:10.1210/jc.2015-1966
- Ramírez F, Dündar F, Diehl S, Grüning BA, Manke T. 2014. deepTools: a flexible platform for exploring deep-sequencing data. *Nucleic Acids Res* **42**: W187–W191. doi:10.1093/nar/gku365
- R Core Team. 2022. *R: a language and environment for statistical computing*. R Foundation for Statistical Computing, Vienna. <https://www.R-project.org/>.
- Robinson MD, McCarthy DJ, Smyth GK. 2010. edgeR: a Bioconductor package for differential expression analysis of digital gene expression data. *Bioinformatics* **26**: 139–140. doi:10.1093/bioinformatics/btp616
- Robinson JT, Thorvaldsdóttir H, Winckler W, Guttman M, Lander ES, Getz G, Mesirov JP. 2011. Integrative genomics viewer. *Nat Biotechnol* **29**: 24–26. doi:10.1038/nbt.1754
- Rolyan H, Tyurina YY, Hernandez M, Amoscato AA, Sparvero LJ, Nmezi BC, Lu Y, Estéicio MR, Lin K, Chen J, et al. 2015. Defects of lipid synthesis are linked to the age-dependent demyelination caused by Lamin B1 overexpression. *J Neurosci* **35**: 12002–12017. doi:10.1523/JNEUROSCI.1668-15.2015
- Rozowsky J, Euskirchen G, Auerbach RK, Zhang ZD, Gibson T, Bjornson R, Carriero N, Snyder M, Gerstein MB. 2009. PeakSeq enables systematic scoring of ChIP-seq experiments relative to controls. *Nat Biotechnol* **27**: 66–75. doi:10.1038/nbt.1518
- Segovia-Miranda F, Morales-Navarrete H, Kücken M, Moser V, Seifert S, Repnik U, Rost F, Brosch M, Hendricks A, Hinz S, et al. 2019. Three-dimensional spatially resolved geometrical and functional models of human liver tissue reveal new aspects of NAFLD progression. *Nat Med* **25**: 1885–1893. doi:10.1038/s41591-019-0660-7
- Shackleton S, Lloyd DJ, Jackson SN, Evans R, Niermeijer MF, Singh BM, Schmidt H, Brabant G, Kumar S, Durrington PN, et al. 2000. LMNA, encoding lamin A/C, is mutated in partial lipodystrophy. *Nat Genet* **24**: 153–156. doi:10.1038/72807

- Sun Z, Miller RA, Patel RT, Chen J, Dhir R, Wang H, Zhang D, Graham MJ, Unterman TG, Shulman GI, et al. 2012. Hepatic Hdac3 promotes gluconeogenesis by repressing lipid synthesis and sequestration. *Nat Med* **18**: 934–942. doi:10.1038/nm.2744
- Tateishi K, Okada Y, Kallin EM, Zhang Y. 2009. Role of Jhdmd2a in regulating metabolic gene expression and obesity resistance. *Nature* **458**: 757–761. doi:10.1038/nature07777
- Varela J, Cadiñanos J, Pendás AM, Gutiérrez-Fernández A, Folgueras AR, Sánchez LM, Zhou Z, Rodríguez FJ, Stewart CL, Vega JA, et al. 2005. Accelerated ageing in mice deficient in Zmpste24 protease is linked to p53 signalling activation. *Nature* **437**: 564–568. doi:10.1038/nature04019
- Villeneuve LM, Reddy MA, Lanting LL, Wang M, Meng L, Natarajan R. 2008. Epigenetic histone H3 lysine 9 methylation in metabolic memory and inflammatory phenotype of vascular smooth muscle cells in diabetes. *Proc Natl Acad Sci* **105**: 9047–9052. doi:10.1073/pnas.0803623105
- Wang L, Xu S, Lee JE, Baldrige A, Grullon S, Peng W, Ge K. 2013. Histone H3K9 methyltransferase G9a represses PPAR $\gamma$  expression and adipogenesis. *EMBO J* **32**: 45–59. doi:10.1038/emboj.2012.306
- Wang J, Yan W, Peng X, Jiang Y, He L, Peng Y, Chen X, Ye M, Zhuo H. 2018. Functional role of SUV39H1 in human renal tubular epithelial cells under high-glucose ambience. *Inflammation* **41**: 1–10. doi:10.1007/s10753-017-0657-7
- Whitton H, Singh LN, Patrick MA, Price AJ, Osorio FG, López-Otín C, Bochkis IM. 2018. Changes at the nuclear lamina alter binding of pioneer factor Foxa2 in aged liver. *Aging Cell* **17**: e12742. doi:10.1111/ace1.12742
- Xu S, Grullon S, Ge K, Peng W. 2014. Spatial clustering for identification of ChIP-enriched regions (SICER) to map regions of histone methylation patterns in embryonic stem cells. *Methods Mol Biol* **1150**: 97–111. doi:10.1007/978-1-4939-0512-6\_5
- Zambelli F, Pesole G, Pavesi G. 2013. PscanChIP: finding over-represented transcription factor-binding site motifs and their correlations in sequences from ChIP-Seq experiments. *Nucleic Acids Res* **41**: W535–W543. doi:10.1093/nar/gkt448
- Zhang L, Rubins NE, Ahima RS, Greenbaum LE, Kaestner KH. 2005. Foxa2 integrates the transcriptional response of the hepatocyte to fasting. *Cell Metab* **2**: 141–148. doi:10.1016/j.cmet.2005.07.002

Received July 25, 2022; accepted in revised form November 16, 2022.